From Fixed to Automated Mirror Arrays: Advancing Multi-Satellite Image Registration Toward Operational Harmonization

Hussain M.D.I. [1*], Nagai M.[1], Katiyar V.[2] and Ichikawa D.[2]

[1]Graduate School of Sciences and Technology for Innovation, Yamaguchi University, Japan

[2]New Space Intelligence Inc., Japan

*danieliman9897@gmail.com

***Abstract*:** *Accurate alignment of satellite imagery across different sensors and spectral bands is critical for reliable multi-source remote sensing applications. Building on our previous work that identified a Fourier-based hybrid co-registration method—combining mirror arrays with local refinement—as the most effective strategy, this study focuses on extending the method to support high-accuracy registration across multiple satellites and imaging conditions. We evaluate a newly developed automated mirror array system that uses TLE-based satellite tracking and dynamic signal adjustment via variable mirror sizes to accommodate spatial resolutions from 15 m to 0.5 m. Compared to the previously used fixed mirror arrays, the automated system requires no manual setup or repositioning and ensures more consistent, real-time alignment with satellite overpasses. The hybrid co-registration method is applied to imagery from Sentinel-2, PlanetScope, and GRUS-1 satellites, targeting both inter-satellite co-registration and intra-satellite band-to-band registration. We quantitatively assess improvements in registration accuracy using RMSE and CE90 metrics, and qualitatively validate results using the Global Reference Image (GRI). A practical case study is demonstrated to illustrate the impact of improved registration on downstream analysis, where misalignment between high and medium resolution images may lead to inaccurate change detection. Results show that the automated mirror array improves geometric consistency across sensors and enhances the interpretability of stacked multi-temporal data. The findings underscore the potential operational advantages of automated mirror arrays as scalable ground references for the harmonization of multi-satellite imagery, facilitating more accurate Earth observation and downstream applications such as environmental monitoring and urban analysis. This work also lays the foundation for future research into integrated radiometric calibration and automated calibration pipelines for emerging microsatellite constellations.*

Keywords: satellite image registration, mirror array, multi-sensor harmonization, microsatellites

Introduction

Accurate geometric alignment of satellite imagery is a critical prerequisite for many remote sensing applications, including land cover change detection, multi-temporal analysis, and multi-sensor data fusion (Samadzadegan et al., 2024). As Earth observation data proliferates—particularly from emerging commercial microsatellite constellations—the challenge of harmonizing spatial discrepancies across sensors has become increasingly urgent. Imagery from different platforms often suffers from sub-pixel misalignments, both

globally and between spectral bands. These misregistrations propagate into downstream analyses, introducing artifacts or misleading patterns that compromise both scientific reliability and operational usability. The Harmonized Landsat and Sentinel-2 (HLS) is one of the leading "virtual constellation" efforts that aim to address this problem and generate analysis-ready, harmonized datasets (Claverie et al., 2018). However, a key bottleneck remains the absence of a universally applicable and automated ground reference system for achieving high-accuracy geometric harmonization across heterogeneous satellite systems.

Artificial ground reference targets have recently gained attention as a promising alternative to traditional ground control points (GCPs), which are often difficult to deploy or maintain in a consistent, high-precision manner. Our previous work (Iman bin Hussain et al., 2025) introduced the use of fixed mirror arrays as high-contrast, point-like reflectors that serve as reliable reference features for satellite image co-registration. Coupled with a hybrid co-registration strategy—combining phase correlation in the frequency domain with global and local co-registration using AROSICS—this approach achieved sub-pixel alignment accuracy across multiple sensors and spectral bands.

However, the fixed mirror array design posed several limitations: it required manual repositioning for each satellite pass, lacked adaptability to different satellite viewing geometries and ground sampling distances (GSDs), and did not support real-time adjustments based on orbital variations. As modern satellites now offer a wide range of spatial resolutions, there is a growing need for a more flexible and scalable ground reference solution. While artificial targets have shown promise, their operational adoption has been hindered by a lack of scalable, automated systems capable of supporting the high-frequency operations of modern satellite constellations, which this research aims to address.

To overcome these operational constraints, we propose and evaluate a newly developed automated mirror array system, designed to support unattended, high-accuracy image registration across a variety of satellite missions. The system integrates Two-Line Element (TLE)-based satellite tracking to dynamically orient mirrors in real-time, while incorporating variable-sized mirrors to optimize signal strength across satellites with GSDs ranging from 15 m to 0.5 m. Unlike the fixed array, this automated system can accommodate successive satellite passes without physical intervention, ensuring consistent visibility under varying lighting and atmospheric conditions.

We apply our validated hybrid co-registration method to datasets from Sentinel-2, PlanetScope, and GRUS-1 satellites, targeting both inter-satellite co-registration and intra-satellite band-to-band alignment. Registration accuracy is quantitatively evaluated using RMSE and CE90 metrics and qualitatively validated against a highly accurate global dataset. We also demonstrated the impact of improved co-registration on downstream applications, such as change detection. The automated mirror array is shown to improve geometric consistency across sensors, enhance the reliability of multi-temporal data, and facilitate scalable harmonization workflows suitable for next-generation Earth observation missions.

It is the first automated mirror array system in Asia specifically designed for real-time geometric referencing based on orbital predictions. Deployed in Yamaguchi, Japan, the system was tested under multiple satellite overpasses, confirming its scalability across different spatial resolutions and sensor types. This approach lays the foundation for future integration with automated radiometric calibration pipelines and operational ground stations, supporting diverse applications from vegetation monitoring to post-disaster assessment.

Literature Review

a. Image Co-Registration Methods

Image registration involves aligning two or more images so that corresponding pixels represent the same location on the ground, and are broadly divided into feature-based and area-based methods. Feature-based algorithms such as SIFT, SURF or ORB (Bay et al., 2006; Fischer et al., 2015; Rublee et al., 2011) detect salient points (e.g., corners, edges), and estimate geometric transforms. Area-based methods compute similarity metrics (e.g., cross-correlation, mutual information) within matching window pairs and derive pixel shifts (Chen et al., 2003; Lewis, 1994). Recent surveys highlight advances in combining feature extraction with deep learning and attention mechanisms to robustly match multimodal or multi-resolution imagery (Xinghua et al., 2023). While deep learning methods show promise, they typically require large, diverse training datasets and significant computational resources, making them less suitable for the rapid, operational deployment envisioned for an automated ground reference system.

Fourier phase correlation is a common area-based technique that efficiently estimates translational shifts between images, noted for its robustness to radiometric differences and noise (Brigham & Morrow, 1967; Tong et al., 2019). Several open-source software have been introduced such as AROSICS that automates the co-registration process by employing Fourier phase correlation on a dense grid of tie points and extensive filtering levels (Scheffler et al., 2017). In our previous work, we combined AROSICS to form a hybrid global-to-local approach, achieving sub-pixel alignment between GRUS-1 and Sentinel-2 imagery.

Despite these advances, registration accuracy often depends on the presence of sufficient image texture and invariant features. When integrating data across different resolutions or sensors, the number of common features can be limited, leading to residual misregistration. A reliable, high-contrast ground reference can greatly simplify the registration problem by providing a well-defined control point that appears in all images.

b. Mirror-Based Calibration Targets

Mirror arrays are novel artificial targets that reflect sunlight toward a satellite, creating a bright specular point in the imagery. Specular reflectors were initially proposed for absolute radiometric calibration (Schiller & Silny, 2010). Other researchers have showed that a fixed mirror array could serve as an artificial point source, enabling accurate radiometric correction and sub-pixel co-registration of micro-satellite imagery (Ichikawa et al., 2022). Additionally, calibration facilities utilizing point-source reflectors for optical satellite data were also developed in Japan, primarily focusing on radiometric calibration (Nagai et al., 2022; Tamkuan et al., 2022). Although successful, the fixed array required repositioning for each pass, did not adapt to different GSDs and could only handle one satellite at a time.
Mirror arrays were also evaluated as part of the BigMAC campaign for Landsat surface product validation, noting deployment challenges but affirming the potential of mirror reflectors (Helder et al., 2025). These studies collectively suggest that mirrors can provide stable radiometric and geometric references, but operationalization remains a challenge.

Methodology

a. Automated Mirror Array

The automated mirror array (called FLARE Lantern) was developed by Labsphere Inc. (New Hampshire, USA) and managed by New Space Intelligence Inc. (Yamaguchi, Japan). It is a portable, automated on-demand calibration system, consisting of convex mirrors, designed for vicarious calibration of high, medium and low spatial resolution sensors by utilizing the SPecular Array Radiometric Calibration (SPARC) method, and is part of the FLARE Vicarious Calibration Network (Russell et al., 2020; Russell et al., 2023.). Consisting of a turret and controller assembly, the Lantern station is specifically designed to cater to sensors with GSDs ranging from 0.5 m to 15 m by configuring variable signal strength levels using different numbers of large and small convex mirrors placed on a flat plate made up of two halves that open up during operations and close when not in use. The turret assembly includes the rotating turret and tripod stand that supports the pivoting mirror arrays. The controller assembly locally provides AC power and control data. Additionally, the turret is also equipped with an embedded solar radiometer, spectrometer and star tracking camera. Figure 1 shows the turret assembly of the automated mirror array.

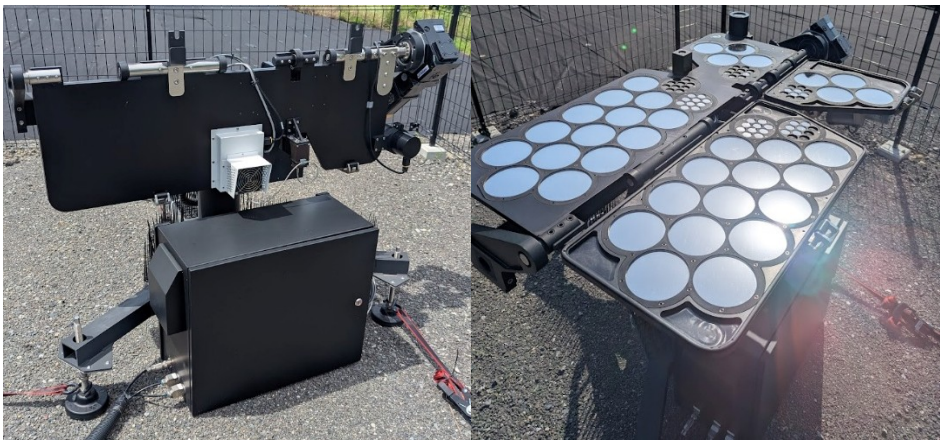

Figure 1: The automated mirror array turret assembly when closed (left) and open (right).

The mirror array is located in Ube City, Yamaguchi Prefecture, Japan. The site is unobstructed, with clear sky visibility and minimal surrounding structures, and the surrounding surfaces are covered with dark-colored materials that emit low reflectance to reduce external effects. TLE data is automatically acquired from Celestrak and processed using the SGP4/SDP4 propagation model to predict satellite observation windows are computed to generate geodetic waypoints (latitude, longitude, altitude) of a specified satellite passing overhead.

b. Data Sources

Data of successful mirror observations from Sentinel-2, PlanetScope and GRUS-1 satellites were acquired in January and February 2025. Each image selected had low cloud cover and clear conditions to minimize any atmospheric effects. Surface reflectance products were acquired for each: Sentinel-2 L2A (MSI) data downloaded from the Copernicus Open Access Hub, PlanetScope SuperDove data (PSB.SD) obtained via Planet Explorer, and GRUS-1 L2A data were provided by Axelspace Corporation (Tokyo, Japan). Only corresponding bands (Blue, Green, Red, NIR) were used.

For inter-sensor co-registration, the red band of each satellite was used and Sentinel-2 was used as reference (when available) due to having an absolute geolocation accuracy of 8 m CE95 and a multi-temporal co-registration accuracy of 5 m CE95 (Rengarajan et al., 2024). Else, the dataset with higher geolocation accuracy is used as reference. For intra-sensor (band-to-band) co-registration, the co-registered red band of each target satellite was used as reference when aligning the other bands (Blue, Green, NIR).

Two acquisition windows were selected (Table 1):

- **January (consecutive):** PSB.SD (23 January), GRUS-1 (24 January), Sentinel-2 (25 January).
- **March (same-day pair):** GRUS-1 + PSB.SD (25 March), Sentinel-2 + PSB.SD (26 March).

Table 1: Data used for this study.

Date	Satellite / Sensor	Spatial resolution
2025-01-23	PSB.SD	3 m
2025-01-24	GRUS-1D	5 m
2025-01-25	Sentinel-2C	10 m
2025-03-25	GRUS-1A	5 m
	PSB.SD	3 m
2025-03-26	Sentinel-2C	10 m
	PSB.SD	3 m

Additionally, the Global Reference Image (GRI) of the study area was also used for further validation after co-registration. GRI is a highly accurate, freely available global dataset, generated by the Institut Géographique National (IGN) and developed by the European Space Agency (ESA) to enhance the absolute and relative geolocation accuracy of multi-temporal Sentinel-2 imagery, consisting of nearly cloud-free, mono-spectral (red band) Sentinel-2 images with an absolute geolocation accuracy of <7 m globally (Gascon et al., 2017).

c. Hybrid Co-registration Procedure

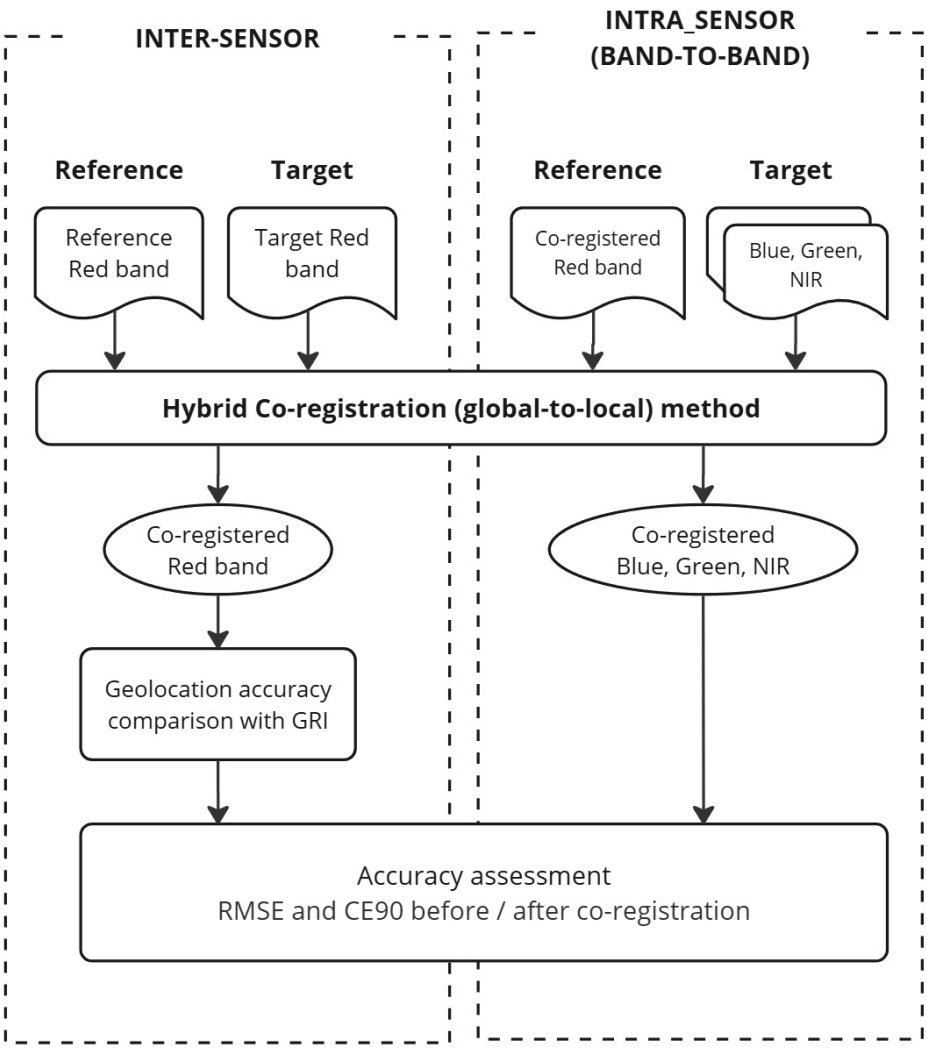

Figure 2: Research methodology overview for inter-sensor and intra-sensor co-registration.

Our approach follows the **hybrid global-to-local method** established in our previous work. The global method utilizes the mirror array, and globally shifts the target band to match the reference band. Afterwards, the local method further refines the accuracy by automatically detecting matching tie points, filtering them through a five-step validation process, computing and applying translational shifts to the target band using cubic convolution (and default parameters). Figure 2 illustrates the applied research methodology. Additionally, a visual assessment was also performed to qualitatively confirm the results.

d. Accuracy Assessment

A comparison of root mean square (RMSE) and circular error at 90th percentile (CE90) errors of detected displacements before and after co-registration was conducted to quantitatively evaluate co-registration accuracy. Displacements were calculated as the absolute shifts between corresponding points in the reference and target bands. The RMSE were computed using the formula: (Eq. 1).

$$\boldsymbol{RMSE} = \sqrt{\frac{\sum_{i=1}^{n}(s_i^2)}{n}} \quad (1)$$

where $\boldsymbol{s_i^2}$ represents the absolute displacement of the $\boldsymbol{i}$-th tie point, and $\boldsymbol{n}$ is the total number of valid tie points included in the calculation. CE90 is computed as the RMSE errors at 90th percentile. For geolocation accuracy, co-registered images were compared to the GRI.

e. Change Detection via NDVI and NDWI

The significance of improved registration on downstream analyses is further demonstrated via a change detection case study. Two application targets were selected: (i) a medium-sized lake/reservoir and (ii) a large-area photovoltaic (PV) installation (solar farm), as shown in Figure 3. Both AOIs exceed several hectares, ensuring meaningful measurement even at Sentinel-2's 10 m grid.

Figure 3: AOI for both solar farm (solar AOI, true color Sentinel-2 image) and lake area (lake AOI, false color Sentinel-2 image).

Change detection was computed by first computing the Normalized Difference Vegetation Index (NDVI) and Normalized Difference Water Index (NDWI) for both PlanetScope and GRUS-1 images before and after co-registration, with Sentinel-2 as the reference, using the equations below:

$$\boldsymbol{NDVI} = \sqrt{\frac{\boldsymbol{NIR - Red}}{\boldsymbol{NIR + Red}}} \quad (2)$$

$$\boldsymbol{NDWI} = \sqrt{\frac{\boldsymbol{Green - NIR}}{\boldsymbol{Green + NIR}}} \quad (3)$$

To isolate geometric effects while minimizing sensitivity to inter-sensor radiometry, we compared each sensor to Sentinel-2 using absolute differences of standard indices rather than the indices themselves. All images were resampled to a common 10 m grid anchored to Sentinel-2 to ensure pixel-to-pixel comparability.

For each AOI we formed per-pixel discrepancies ΔNDVI = |NDVIsensor – NDVIs2| or ΔNDWI = |NDWIsensor – NDWIs2|, and then summarized them with the mean and standard deviation inside the AOI. Percentage improvement was reported after co-registration as:

$$\boldsymbol{\Delta}(\%) = \sqrt{\frac{\boldsymbol{Before - After}}{\boldsymbol{Before}}}\ \boldsymbol{x\ 100} \quad (4)$$

for both statistics. AOIs included class boundaries (shoreline for water, perimeter/roads for the solar farm), where geometric misalignment most strongly affects |Δ|. No radiometric or spectral harmonization was applied, by design, so that any reduction in |Δ| reflects improved spatial harmonization.

Results and Discussion

a. Inter-sensor Co-registration Accuracy

Figure 4 and Figure 5 illustrates the geolocation accuracy before and after co-registration for both January and March blocks.

(a) Sentinel-2 – PlanetScope (January)

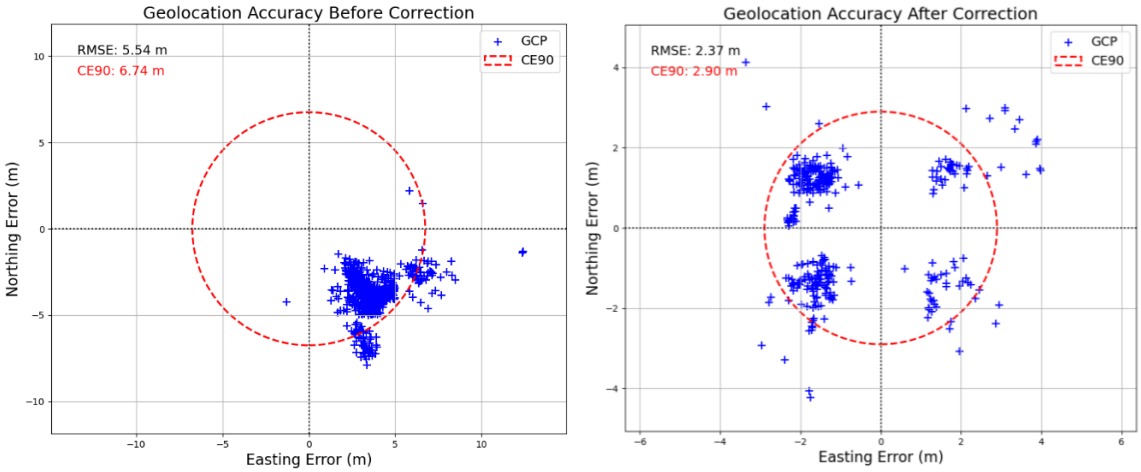

(b) Sentinel-2 – GRUS-1 (January)

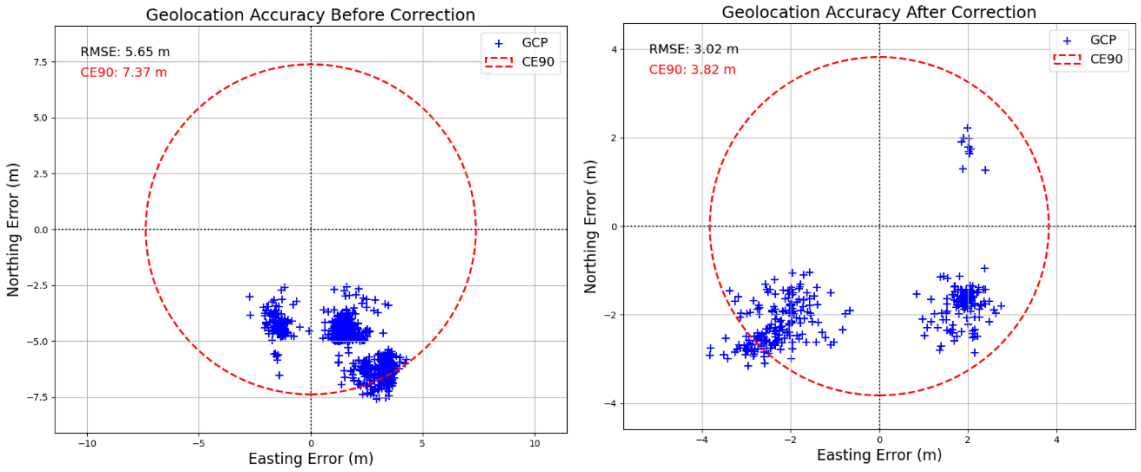

Figure 4: Geolocation accuracy before and after co-registration for January; (a) Sentinel-2 – PlanetScope, (b) Sentinel-2 – GRUS-1

For the January block, prior to co-registration, Planet and GRUS-1 exhibited values of 5.54 m RMSE (6.74 m CE90) and 5.65 m RMSE (7.37 m CE90), respectively, relative to the reference Sentinel-2 imagery (Figure 4). After applying the automated mirror array hybrid correction, errors were reduced to 2.37 m RMSE (2.9 m CE90) for Planet and 3.02 m RMSE (3.82 m CE90) for GRUS-1. These reductions represent approximately a 50 percent improvement, with final errors consistently within half a Sentinel-2 pixel. This ~50% reduction in error demonstrates the system's ability to correct for typical orbital uncertainties and sensor pointing variations, anchoring the higher-resolution imagery to the globally consistent Sentinel-2 grid.

(a) PlanetScope – GRUS-1 (March)

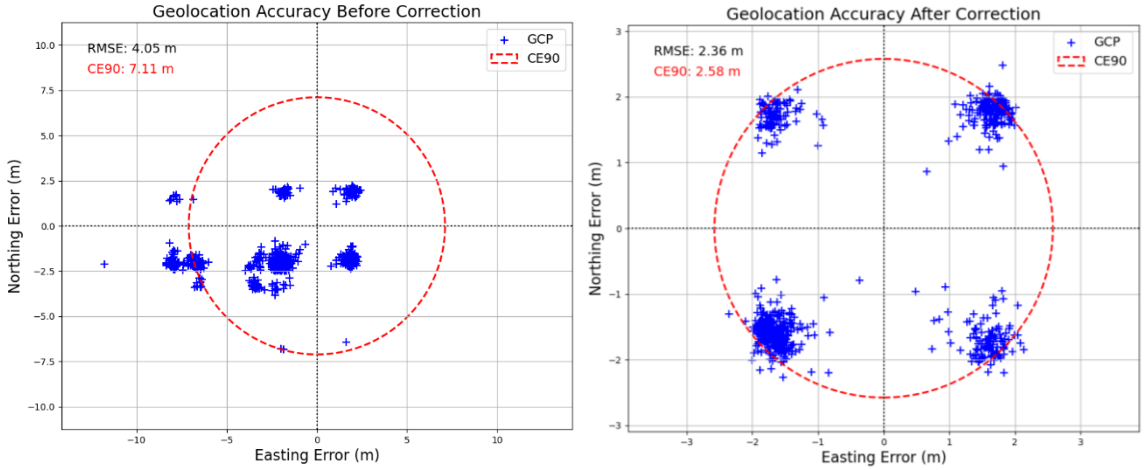

(b) Sentinel-2 – PlanetScope (March)

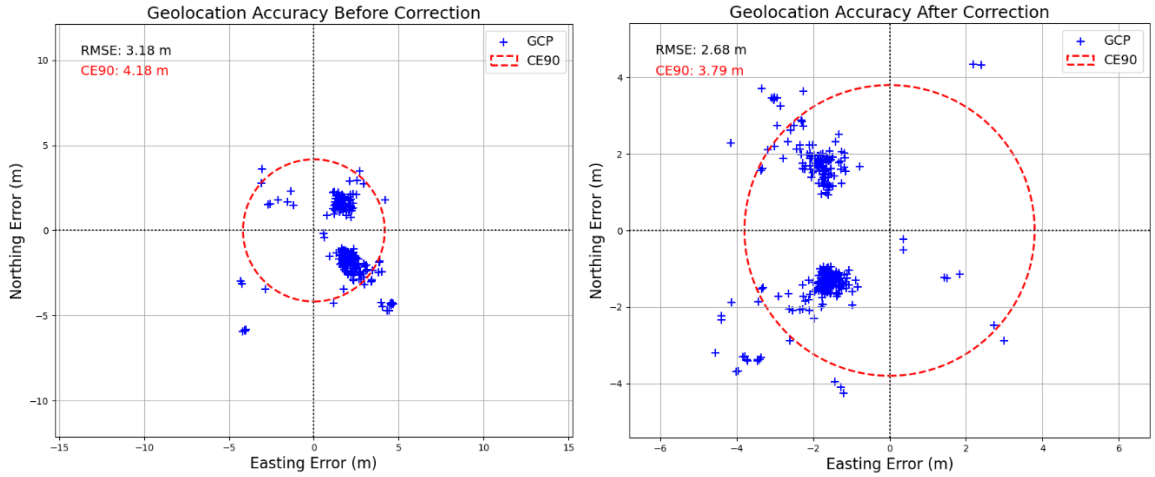

Figure 5: Geolocation accuracy before and after co-registration for March; (a) PlanetScope – GRUS-1, (b) Sentinel-2 – PlanetScope

The March block offered an opportunity to validate the approach under near-simultaneous conditions. Planet and GRUS were acquired on 25 March, followed by Planet and Sentinel-2 on 26 March (Figure 5). Before correction, Planet–GRUS images showed values of 4.05 m RMSE (7.11 m CE90). After mirror-based alignment, these improved substantially to 2.36 m RMSE (2.58 m CE90). For Planet–Sentinel pairs, the initial misalignment was smaller (3.18 m RMSE, 4.18 m CE90), and the gains after correction were more modest, with final values of 2.68 m and 3.79 m, respectively. Even in this case, however, the alignment was tightened to within 0.3 pixels of Sentinel-2.

Table 2 shows a summary of the inter-sensor co-registration results for each image pair.

Table 2: Summary of the inter-sensor co-registration results

Reference (Date)	**Target (Date)**	**RMSE (CE90) before (m)**	**RMSE (CE90) after (m)**
Sentinel-2 (2025-01-25)	PlanetScope (2025-01-23)	5.54 (6.74)	2.37 (2.9)
	GRUS-1 (2025-01-24)	5.65 (7.37)	3.02 (3.82)
PlanetScope (2025-03-25)	GRUS-1 (2025-03-25)	4.05 (7.11)	2.36 (2.58)
Sentinel-2 (2025-03-26)	PlanetScope (2025-0-26)	3.18 (4.18)	2.68 (3.79)

Visual assessment of the co-registered imagery confirms the quantitative results. Figure 6 shows before-and-after image overlays between each image pair. In the overlays, the red channel represents the target image and the green channel represents the reference image. The resulting composite follows the image with the lower spatial resolution.

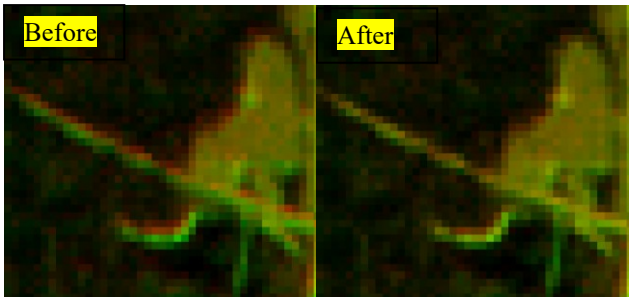

(a) Sentinel-2 – PlanetScope (road)

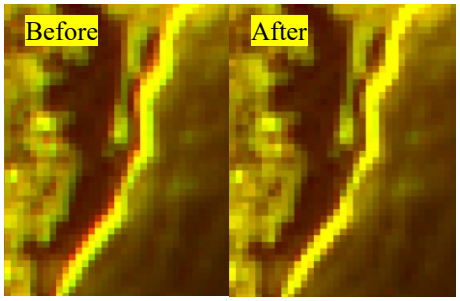

(b) Sentinel-2 – GRUS-1 (coastline)

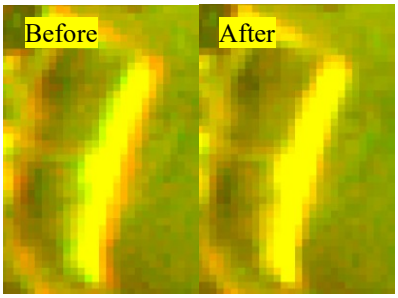

(c) PlanetScope – GRUS-1 (coastline)

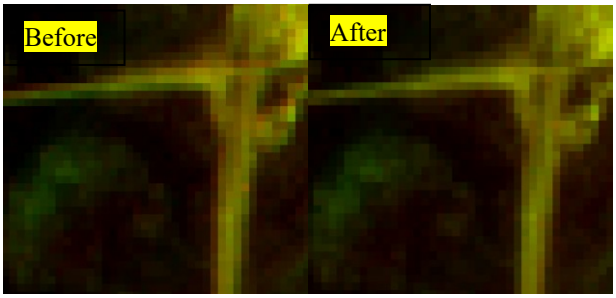

(d) Sentinel-2 – PlanetScope (road)

Figure 6: Two-band image overlay of each image pair before and after co-registration.

Before co-registration, misalignments are visible, and seen as red and green "fringes" surrounding features such as roads and coastlines. This is also called the "rainbow" effect, which is commonly seen in multiband images with poor band-to-band accuracy. After co-registration, this effect is effectively reduced, leading to greater alignment.

By aligning Planet and GRUS-1 to Sentinel-2, which itself is tied to the Global Reference Image (GRI), consecutive and same-day acquisitions effectively behaved as a seamless virtual constellation. This provides direct evidence that automated mirror arrays can enable multi-sensor data streams to be treated as interchangeable temporal observations.

b. Intra-sensor (Band-to-Band) Co-registration Accuracy

For band-to-band co-registration, the RMSE values before and after co-registration for each band were calculated (Figure 7).

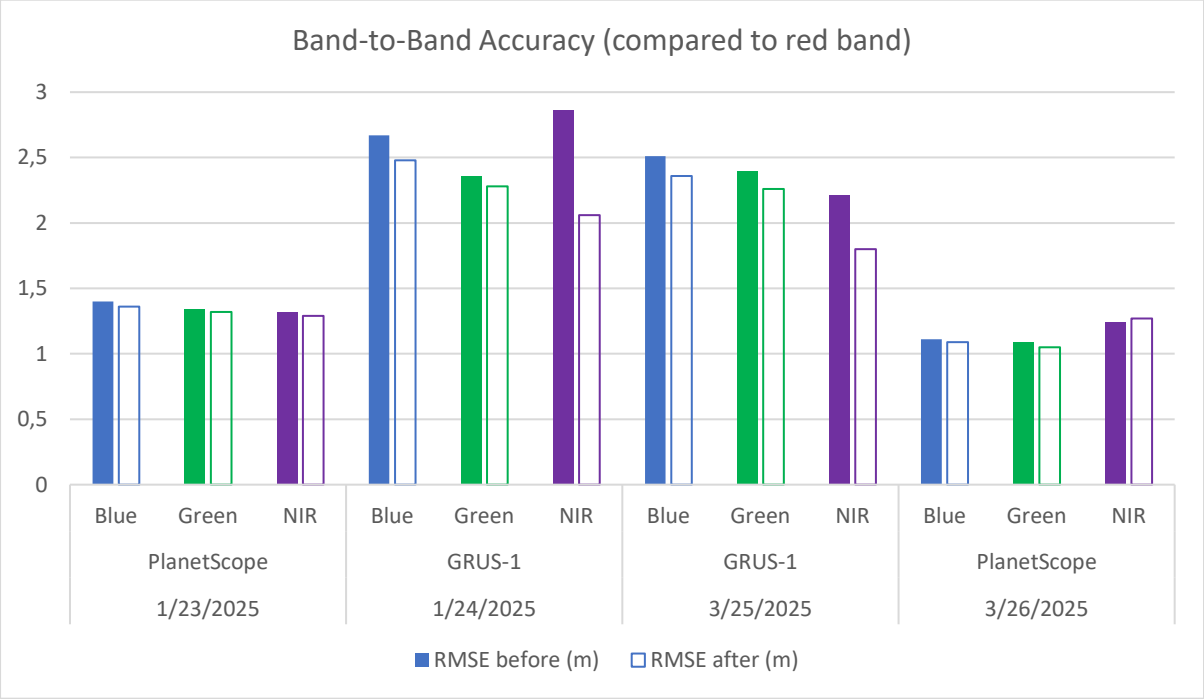

Figure 7: Band-to-band accuracy before and after co-registration for each band (except the red band that was used as the reference band)

For GRUS-1, band-to-band accuracy relative to the red band were initially on the order of 2.2–2.9 m, with the NIR band occasionally exhibiting larger deviations (up to 2.86 m RMSE). After correction, RMSE values decreased by 0.3–0.6 m across bands, with the NIR band reduced to 2.34 m and CE90 to 2.65 m.

PlanetScope, in contrast, already demonstrated excellent band-to-band alignment, with RMSE values around 1.1–1.4 m (less than half a PlanetScope pixel) before correction and only marginal changes afterward. This confirms Planet's strong internal calibration, following the band alignment threshold of less than 0.3 pixels for "standard" quality products (PlanetScope, 2025) but also demonstrates that the mirror-based workflow can verify and, when necessary, refine band-to-band accuracy.

c. Validation with GRI

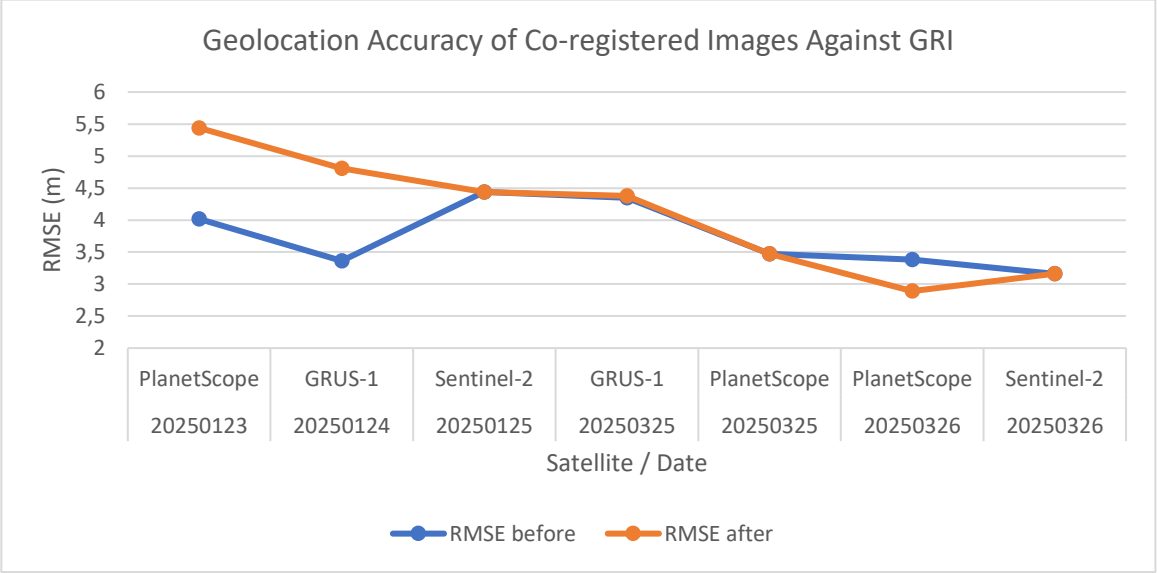

Figure 8: Geolocation accuracy of the co-registered images against GRI for each target satellite, excluding Sentinel-2 and 2025-03-25 PlanetScope imagery.

Validation against the GRI revealed important differences between the January and March datasets (Figure 7). In January, Planet (23 Jan) and GRUS (24 Jan) were co-registered to Sentinel-2 (25 Jan). Relative alignment between the three sensors improved, but absolute accuracy with respect to the GRI did not. PlanetScope's RMSE increased from 4.02 m to 5.44 m (5.08 m to 6.54 m CE90), while GRUS-1 worsened from 3.36 m to 4.81 m RMSE (4.61 m to 5.31 m CE90). The Sentinel-2 image itself exhibited an RMSE of 4.44 m (CE90 of 5.35 m), confirming that this acquisition was not tightly aligned to the GRI. Consequently, using this Sentinel-2 scene as the reference propagated its misregistration into the corrected Planet and GRUS-1 images.

By contrast, the March block showed more promising outcomes. On 25 March, GRUS-1

had an RMSE of 4.35 m relative to the GRI, which remained stable after correction (4.38 m), while PlanetScope's accuracy was already good at 3.47 m RMSE. On 26 March, PlanetScope improved from 3.38 m to 2.89 m RMSE (3.83 m to 3.71 m CE90) after co-registration, demonstrating that alignment to a well-registered Sentinel-2 scene enhanced its absolute accuracy. Sentinel-2 on the same date showed 3.16 m RMSE and 3.92 m CE90, confirming that this acquisition was closely aligned to the GRI. These results illustrate that when Sentinel-2 imagery is accurately tied to the GRI, the automated mirror array method can both harmonize relative geometry and improve absolute geolocation accuracy. Conversely, when the chosen reference is less accurate, the target imagery inherits its biases.

Overall, these findings highlight that the choice of reference image is critical in mirror-based co-registration workflows. Sentinel-2 provides a globally consistent reference system, but individual acquisitions vary in accuracy. A practical strategy is therefore to validate candidate reference images against the GRI before applying them in multi-sensor harmonization. This ensures that the benefits of relative co-registration are not offset by degradation in absolute positioning.

d. Change Detection Results

Across both AOIs, co-registration consistently reduced cross-sensor disagreement with Sentinel-2, most clearly in the variability (standard deviation) of |Δ|, which is dominated by edge pixels (Table 3).

Table 3: Mean, standard deviation and Δ (%) values before and after co-registration for each AOI and satellite

Satellite	AOI	Metric	Before	After	Δ (%)
PlanetScope	Lake	Mean	0.199	0.198	0.14
	Lake	Std	0.062	0.054	13.28
	Solar	Mean	0.169	0.167	0.90
	Solar	Std	0.05	0.048	3.38
GRUS-1	Lake	Mean	0.168	0.1678	0.09
	Lake	Std	0.074	0.073	0.28
	Solar	Mean	0.078	0.0732	6.52
	Solar	Std	0.059	0.056	4.77

Across both AOIs, co-registration consistently reduced cross-sensor disagreement with Sentinel-2, most clearly in the variability (standard deviation) of |Δ|, which is dominated by edge pixels. For PlanetScope over the water AOI, the standard deviation of |ΔNDWI| fell from 0.0620 to 0.0538 (≈13.3% improvement), while the mean decreased marginally from 0.19860 to 0.19832 (≈0.14%). Over the solar AOI, PlanetScope showed a smaller but still clear reduction in variability (std 0.04993 to 0.04824, ≈3.38% improvement) and a modest decrease in the mean cross-sensor difference (0.9039%). These patterns match expectations: most pixels in these AOIs are homogeneous (open water or panel arrays), so the mean |Δ| moves little, while the spread tightens as edge jitter is removed.

GRUS-1 shows the same direction of change, with smaller magnitudes in the water AOI (std 0.07377 to 0.07357, ≈0.28%; mean 0.0897% improvement), and a stronger response in the solar AOI (mean 0.07828 to 0.07318, ≈6.52%; std 0.05940 to 0.05656, ≈4.77%). The comparatively larger improvement of GRUS over the solar AOI suggests that, prior to co-registration, small misalignments against the high-contrast PV boundaries contributed measurably to the Planet/GRUS–S2 discrepancies; after co-registration those edge-driven discrepancies contracted. The very small changes in the water-AOI means (≈0.1%) are not surprising and should be interpreted as stability, not lack of benefit: interior open water contributes many low-variance pixels that dilute the mean, while the geometric gains appear primarily as a reduction in dispersion near the shoreline.

Taken together, these results support the core claim: mirror-based co-registration primarily improves spatial agreement between heterogeneous sensors rather than shifting overall index levels. By measuring mean(|Δ|) and std(|Δ|) against a common Sentinel-2 grid, we see reductions of ≈3–13% in variability where edges matter most, alongside small but consistent declines in average discrepancy. Residual differences after alignment are expected due to sensor spectral response, BRDF, and any remaining absolute geolocation error in the Sentinel-2 anchor; however, the observed tightening of |Δ| distributions indicates that geometry—not radiometry—was the limiting factor before co-registration.

e. Limitations

While promising, the method has some limitations. The mirror signal requires clear skies and direct sunlight; heavy cloud cover or haze can obscure the reflection, preventing

detection. Incorporating redundancy (e.g., multiple mirrors or multiple passes) and scheduling imaging during clear periods can mitigate this issue. The system currently handles only specular reflections; integrating a Lambertian reflector or diffuse panel could provide additional radiometric calibration functionality, although this is beyond the scope of this paper.

The automated system introduces mechanical complexity: motors and control electronics must be weather-protected and require periodic maintenance. Accurate timing and TLE updates are critical to ensure proper alignment. Additionally, deploying multiple such systems globally would necessitate logistical coordination and standardized software. Nonetheless, the operational benefits—unattended calibration, adaptability to multiple satellites and enhanced accuracy—make the approach attractive for large-scale implementation.

Conclusion

This study presents an automated mirror array system that advances previous fixed mirror approaches to multi-sensor image co-registration. By integrating TLE-based satellite tracking, motorized mirror control and variable mirror sizes, the system automatically aligns with satellites of different resolutions and orbits. Combined with a hybrid co-registration algorithm, the method achieves sub-pixel registration across time-series Sentinel-2, PlanetScope and GRUS-1 imagery. Quantitative results (e.g., improvement from ~14 m to ~3 m RMSE for PlanetScope–Sentinel-2 pairs) and qualitative case studies demonstrate that the automated mirror array significantly enhances geometric consistency, thereby improving downstream applications such as change detection.

This work establishes the potential of automated ground references for operational harmonization of emerging microsatellite constellations. Future research will focus on integrating radiometric calibration using the same mirror array, characterizing the sensor point spread function for deblurring, and deploying a network of automated mirror stations to provide global coverage. Combining geometric and radiometric calibration in a unified framework would enable truly analysis-ready multi-sensor datasets. Moreover, exploring machine learning techniques for automatic mirror detection and real-time feedback control may further streamline the calibration process.

Acknowledgement

The authors acknowledge the support of YUCARS and the contributions of colleagues from New Space Intelligence Inc (NSI). We thank Axelspace and Planet Labs for providing the satellite imagery.

References

Bay, H., Tuytelaars, T., & Van Gool, L. (2006). SURF: Speeded Up Robust Features. In A. Leonardis, H. Bischof, & A. Pinz (Eds.), *Computer Vision – ECCV 2006* (pp. 404–417). Springer. https://doi.org/10.1007/11744023_32

Brigham, E. O., & Morrow, R. E. (1967). The fast Fourier transform. *IEEE Spectrum*, *4*(12), 63–70. IEEE Spectrum. https://doi.org/10.1109/MSPEC.1967.5217220

Chen, H.-M., Varshney, P. K., & Arora, M. K. (2003). Performance of mutual information similarity measure for registration of multitemporal remote sensing images. *IEEE Transactions on Geoscience and Remote Sensing*, *41*(11), 2445–2454. IEEE Transactions on Geoscience and Remote Sensing. https://doi.org/10.1109/TGRS.2003.817664

Claverie, M., Ju, J., Masek, J. G., Dungan, J. L., Vermote, E. F., Roger, J.-C., Skakun, S. V., & Justice, C. (2018). The Harmonized Landsat and Sentinel-2 surface reflectance data set. *Remote Sensing of Environment*, *219*, 145–161. https://doi.org/10.1016/j.rse.2018.09.002

Fischer, P., Dosovitskiy, A., & Brox, T. (2015). *Descriptor Matching with Convolutional Neural Networks: A Comparison to SIFT* (arXiv:1405.5769). arXiv. https://doi.org/10.48550/arXiv.1405.5769

Gascon, F., Bouzinac, C., Thépaut, O., Jung, M., Francesconi, B., Louis, J., Lonjou, V., Lafrance, B., Massera, S., Gaudel-Vacaresse, A., Languille, F., Alhammoud, B., Viallefont, F., Pflug, B., Bieniarz, J., Clerc, S., Pessiot, L., Trémas, T., Cadau, E., … Fernandez, V. (2017). Copernicus Sentinel-2A Calibration and Products Validation Status. *Remote Sensing*, *9*(6), Article 6. https://doi.org/10.3390/rs9060584

Helder, D., Shrestha, M., Mann, J., Maddox, E., Irwin, J., Leigh, L., Gerace, A., Eon, R., Falcon, L., Conran, D., Raqueno, N., Bauch, T., Durell, C., & Russell, B. (2025). Landsat Surface Product Validation Instrumentation: The BigMAC Exercise. *Sensors*, *25*(8), 2586. https://doi.org/10.3390/s25082586

Ichikawa, D., Nagai, M., Tamkuan, N., Katiyar, V., Eguchi, T., & Nagai, Y. (2022). Development and Utilization of a Mirror Array Target for the Calibration and Harmonization of Micro-Satellite Imagery. *Remote Sensing*, *14*(22), Article 22. https://doi.org/10.3390/rs14225717

Iman bin Hussain, M. D., Katiyar, V., Nagai, M., & Ichikawa, D. (2025). Enhancing Satellite Image Coregistration Using Mirror Array as Artificial Point Source for Multisource Image Harmonization. *IEEE Journal of Selected Topics in Applied Earth Observations and Remote Sensing*, *18*, 16983–16996. https://doi.org/10.1109/JSTARS.2025.3582238

Lewis, J. P. (1994). Fast Template Matching. *Vis. Interface*, *95*.

Nagai, M., Tamkuan, N., Ichikawa, D., Nagai, Y., Eguchi, T., & Katiyar, V. (2022, March 3). Calibration Facilities and Method Based on Point-Source Reflectors for Optical Satellite Data Application. *The 33rd International Symposium on Space Technology and Science.* The 33rd International Symposium on Space Technology and Science.

PlanetScope | Planet Documentation. (2025, September 11). https://docs.planet.com/data/imagery/planetscope/

Rengarajan, R., Choate, M., Hasan, M. N., & Denevan, A. (2024). Co-registration accuracy between Landsat-8 and Sentinel-2 orthorectified products. *Remote Sensing of Environment*, *301*, 113947. https://doi.org/10.1016/j.rse.2023.113947

Rublee, E., Rabaud, V., Konolige, K., & Bradski, G. (2011). ORB: An efficient alternative to SIFT or SURF. *2011 International Conference on Computer Vision*, 2564–2571. https://doi.org/10.1109/ICCV.2011.6126544

Russell, B., Scharpf, D., Holt, J., Arnold, W., Durell, C., Jablonski, J., Conran, D., Schiller, S., Leigh, L., Aaron, D., & Oliveira, P. V. de C. e. (2020). Initial results of the FLARE vicarious calibration network. *Earth Observing Systems XXV*, *11501*, 44–57. https://doi.org/10.1117/12.2566759

Samadzadegan, F., Toosi, A., & Dadrass Javan, F. (n.d.). A critical review on multi-sensor and multi-platform remote sensing data fusion approaches: Current status and prospects. *International Journal of Remote Sensing*, *0*(0), 1–76. https://doi.org/10.1080/01431161.2024.2429784

Scheffler, D., Hollstein, A., Diedrich, H., Segl, K., & Hostert, P. (2017). AROSICS: An Automated and Robust Open-Source Image Co-Registration Software for Multi-Sensor Satellite Data. *Remote Sensing*, *9*(7), Article 7. https://doi.org/10.3390/rs9070676

Schiller, S. J., & Silny, J. (2010). The Specular Array Radiometric Calibration (SPARC) method: A new approach for absolute vicarious calibration in the solar reflective spectrum. *Remote Sensing System Engineering III*, *7813*, 108–126. https://doi.org/10.1117/12.864071

Tamkuan, N., Ichikawa, D., Katiyar, V., Nagai, Y., Eguchi, T., & Nagai, M. (2022). Optical Multi-Satellite data Calibration for Image Integration and Harmonization. *IGARSS 2022 - 2022 IEEE International Geoscience and Remote Sensing Symposium*, 4595–4598. https://doi.org/10.1109/IGARSS46834.2022.9884814

The Ground to Space CALibration Experiment (G-SCALE): Simultaneous Validation of UAV, Airborne, and Satellite Imagers for Earth Observation Using Specular Targets. (n.d.). Retrieved September 28, 2025, from https://www.mdpi.com/2072-4292/15/2/294

Tong, X., Ye, Z., Xu, Y., Gao, S., Xie, H., Du, Q., Liu, S., Xu, X., Liu, S., Luan, K., & Stilla, U. (2019). Image Registration With Fourier-Based Image Correlation: A Comprehensive Review of Developments and Applications. *IEEE Journal of Selected Topics in Applied Earth Observations and Remote Sensing*, *12*(10), 4062–4081. IEEE Journal of Selected Topics in Applied Earth Observations and Remote Sensing. https://doi.org/10.1109/JSTARS.2019.2937690

Xinghua, L. I., Wenhao, A. I., Ruitao, F., & Shaojie, L. U. O. (2023). Survey of remote sensing image registration based on deep learning. *National Remote Sensing Bulletin*, *27*(2), 267–284. https://doi.org/10.11834/jrs.20235012